ISSN 1674-1056
http://cpb.iphy.ac.cn
http://iopscience.iop.org/cpb
中国物理 B
Chinese Physics
中国物理 Chinese Physics B

Microstructure and ferromagnetism ofheavily Mn doped SiGe thin flims

Huanming Wang(王焕明), Sen Sun(孙森), Jiayin Xu(徐家胤), Xiaowei Lv(吕晓伟), Yuan Wang(汪渊), Yong Peng(彭勇), Xi Zhang(张析), Gang Xiang(向钢)
Citation: Chin. Phys. B . 2020, 29(5): 057504 . **doi:** 10.1088/1674-1056/ab8219
Journal homepage: http://cpb.iphy.ac.cn; http://iopscience.iop.org/cpb

What follows is a list of articles you may be interested in

Two-dimensional XSe_2 (X=Mn, V) based magnetic tunneling junctions with high Curie temperature

Longfei Pan(潘龙飞), Hongyu Wen(文宏玉), Le Huang(黄乐), Long Chen(陈龙), Hui-Xiong Deng(邓惠雄), Jian-Bai Xia(夏建白), Zhongming Wei(魏钟鸣)
Chin. Phys. B . 2019, 28(10): 107504 . **doi:** 10.1088/1674-1056/ab3e45

Effects of chemical pressure on diluted magnetic semiconductor $(Ba,K)(Zn,Mn)_2As_2$

Y Peng(彭毅), S Yu(于爽), G Q Zhao(赵国强), W M Li(李文敏), J F Zhao(赵建发), L P Cao(曹立朋), X C Wang(望贤成), Q Q Liu(刘清青), S J Zhang(张思佳), R Z Yu(于润泽), Z Deng(邓正), X H Zhu(朱小红), C Q Jin(靳常青)
Chin. Phys. B . 2019, 28(5): 057501 . **doi:** 10.1088/1674-1056/28/5/057501

Structural stability at high pressure, electronic, and magnetic properties of BaFZnAs: A new candidate of host material of diluted magnetic semiconductors

Bi-Juan Chen(陈碧娟), Zheng Deng(邓正), Xian-Cheng Wang(望贤成), Shao-Min Feng(冯少敏), Zhen Yuan(袁真), Si-Jia Zhang(张思佳), Qing-Qing Liu(刘清青), Chang-Qing Jin(靳常青)
Chin. Phys. B . 2016, 25(7): 077503 . **doi:** 10.1088/1674-1056/25/7/077503

Room-temperature ferromagnetism induced by Cu vacancies in $Cu_x(Cu_2O)_{1-x}$ granular films

Xie Xin-Jian, Li Hao-Bo, Wang Wei-Chao, Lu Feng, Yu Hong-Yun, Wang Wei-Hua, Cheng Ya-Hui, Zheng Rong-Kun, Liu Hui
Chin. Phys. B . 2015, 24(9): 097504 . **doi:** 10.1088/1674-1056/24/9/097504

Tailoring the structural and magnetic properties of Cu-doped ZnO by *c*-axis pressure

Gong Ji-Jun, Chen Ji-Pei, Zhang Fei, Wu Hao, Qin Ming-Hui, Zeng Min, Gao Xing-Sen, Liu Jun-Ming
Chin. Phys. B . 2015, 24(3): 037505 . **doi:** 10.1088/1674-1056/24/3/037505

Microstructure and ferromagnetism of heavily Mn doped SiGe thin flims*

Huanming Wang(王焕明)[1], Sen Sun(孙森)[2], Jiayin Xu(徐家胤)[1], Xiaowei Lv(吕晓伟)[3], Yuan Wang(汪渊)[2,†], Yong Peng(彭勇)[3], Xi Zhang(张析)[1], and Gang Xiang(向钢)[1,‡]

[1] *College of Physics, Sichuan University, Chengdu* 610064, *China*
[2] *Key Laboratory of Radiation Physics and Technology, Ministry of Education, Institute of Nuclear Science and Technology, Sichuan University, Chengdu* 610064, *China*
[3] *Key Laboratory for Magnetism and Magnetic Materials of Ministry of Education, Lanzhou University, Lanzhou* 73000, *China*

(Received 14 February 2020; revised manuscript received 12 March 2020; accepted manuscript online 23 March 2020)

Heavily Mn-doped SiGe thin films were grown by radio frequency magnetron sputtering and then treated by post-growth thermal annealing. Structural characterizations reveal the coexistence of Mn-diluted SiGe crystals and Mn-rich nanoclusters in the annealed films. Magnetic measurements indicate the ferromagnetic ordering of the annealed samples above room temperature . The data suggest that the ferromagnetism is probably mainly contributed by the Ge-rich nanoclusters and partially contributed by the tensile-strained Mn-diluted SiGe crystals. The results may be useful for room temperature spintronic applications based on group IV semiconductors.

Keywords: Mn-doped SiGe, diluted magnetic semiconductor, nanoclusters, ferromagnetism

PACS: 75.50.Pp, 78.40.Fy, 75.75.–c **DOI:** 10.1088/1674-1056/ab8219

1. Introduction

Diluted magnetic semiconductors (DMSs) have attracted lots of interest in the last two decades due to their potential applications in spintronic devices.[1–11] Substantial works have been carried out to dope transition-metals (TMs) in various semiconductors such as III–V,[1–4] II–VI,[5,6] group-IV,[7,8] and I–II–V[9–11] semiconductors. Among them, Mn doped group-IV semiconductors have drawn considerable attention for their compatibility with current silicon process technology. However, owing to the low solubility of Mn in group-IV semiconductors,[12] the ferromagnetic (FM) nanostructures of manganese silicide[13,14] and manganese germanide[15,16] compounds were usually formed in heavily Mn-doped Ge and Si samples. Such Mn-rich nanostructures embedded in the semiconductors have been obtained through self-organized aggregation[17] and could be an effective way to achieve high T_C spintronic devices.[18] Although extensive studies have been performed on heavily Mn-doped Ge and Si samples,[13–19] no such studies have been reported on the Mn-doped SiGe compound yet. Considering that the SiGe alloy as an important semiconductor has been widely used in high-speed transistors in which the lattice strain and electronic properties are closely related to the alloy components,[20] it will be useful to explore the correlation between the microstructures and magnetic properties of heavily Mn-doped SiGe.

In this work, heavily (above 10%) Mn-doped $Si_{0.25}Ge_{0.75}$ thin films were synthesized by radio frequency (r.f.) magnetron sputtering and then treated by post-growth rapid thermal annealing. The structural characterizations reveal that the Mn diluted SiGe crystals and Mn-rich nanoclusters coexisted in the annealed films, owing to the crystallization and phase separation during the treatment process. The magnetic measurements of the annealed samples show a T_C around room temperature. Further analysis reveals the relationship between the FM ordering and the Mn-rich nanoclusters as well as Mn diluted SiGe crystals in the annealed samples.

2. Experimental details

$Si_{0.25}Ge_{0.75}$:Mn_x thin films ($x = 0.1$ and 0.2) were grown by r.f. magnetron sputtering using 99.999% germanium (Ge) target, 99.999% silicon (Si) target, and 99.99% manganese (Mn) target. We used semi-insulating one-side polished Ge (100) wafers as the substrates. The Ge wafers were first ultrasonically cleaned by using ethanol, acetone, and diluted hydrofluoric acid solution (10%), then flushed by using deionized water, and finally loaded into the growth chamber. The base pressure prior to deposition was about 1.0×10^{-5} Pa. During the deposition, the substrate temperature was kept at 250 ℃. Argon was used as the working gas. A 150 nm $Si_{0.25}Ge_{0.75}$:Mn_x film was deposited on the Ge substrate. After deposition, some samples were annealed at 800 ℃ for 30 s by using a rapid thermal annealing furnace (NBD-HR1200-110IT) in 95% Ar_2/5% H_2 atmosphere.

*Project supported by the National Key R&D Program of China (Grant No. 2017YFB0405702) and the National Natural Science Foundation of China (Grant No. 51671137).

†Corresponding author. E-mail: wyuan@scu.edu.cn
‡Corresponding author. E-mail: gxiang@scu.edu.cn

© 2020 Chinese Physical Society and IOP Publishing Ltd

The films were deposited on Al_2O_3 substrate for detecting the composition by using a field-emission scanning electron microscope (EDAX, X-MaxN 80, Oxford). Grazing incidence x-ray diffraction (GIXRD, Bruker D8, Empyrean Panalytical diffractometer) using a Cu $K\alpha$ radiation source with $\lambda = 0.154$ nm was applied to detect the structural properties of the samples. The vibration modes of the lattice were characterized by Raman spectroscopy using a custom-built confocal micro-Raman optical assembly with a 532 nm laser and an Andor EMCCD detector. Transmission electronic micrograph (TEM, Tecnai F30, FEI) was applied to detect the structural properties. The cross-section samples for the TEM measurement were prepared by a focus ion beam (FIB) milling procedure in a Helios (Tescan, LYRA 3 XMU). Also, the element distribution in our cross-section samples was characterized by using energy dispersive x-ray spectrometry in TEM measurement (EDS, Bruker Super-X, Bruker). The magnetic properties were measured by using a superconducting quantum interference device (SQUID) magnetometer (MPMS XL-7, Quantum Design).

3. Results and discussion

The GIXRD measurements were first performed to study the crystalline structures of the samples. For simplicity, the three representative samples mainly discussed in this work are named as S1 ($x = 0.1$, as-grown), S2 ($x = 0.1$, annealed), and S3 ($x = 0.2$, annealed). As shown in Fig. 1(a), the as-grown sample S1 does not show apparent diffraction peaks, which indicates that the as-grown sample is amorphous. In fact, all the heavily doped as-grown samples studied were amorphous. Meanwhile, the annealed samples S2 and S3 have clear peaks at around 27.6° and 45.9°, indicating that the crystallization of the SiGe diamond phase occurred during the annealing process. All the annealed samples studied showed similar behavior. The SiGe grain sizes of S2 and S3 calculated by the Scherrer formula are 13 nm and 16 nm, respectively. All the $Si_{0.25}Ge_{0.75}$ peak positions of samples S2 and S3 are clearly left-shifted comparing with the unstrained value (Fig. 1(a), red dashed line), indicating the existence of tensile strain in the samples. In the GIXRD patterns of samples S2 and S3, there exist several peaks between 30° and 45°, which come from the Ge_3Mn_5 phase[21] (Fig. 1(a), pink dashed line). The Ge_3Mn_5 peaks show a little shift owing to the grain size reduction induced by Si incorporation in the alloy. No manganese oxides were detected in any of the samples. Also, there are still some peaks (marked by *) that could not be distinguished from various kinds of manganese silicide and manganese germanide.

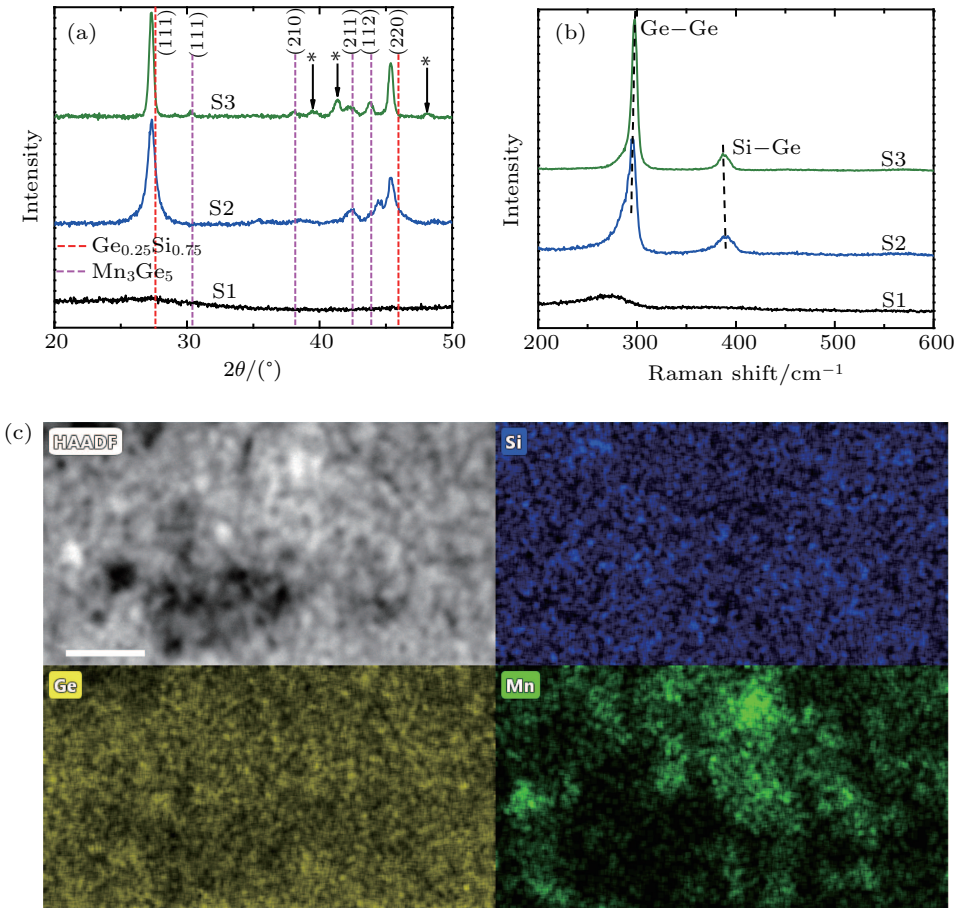


Fig. 1. (a) GIXRD spectra and (b) Raman spectra of samples S1, S2, and S3. (c) HADDF and EDS mapping images for sample S2.

To study the lattice vibration modes, the Raman spectra of samples S1, S2 and S3 were taken. Since the penetration depth of a 532 nm laser in Si or Ge is less than 50 nm, the influence of the Ge substrate could be excluded. As shown in Fig. 1(b), the spectra reveal two main vibrational modes at near 300 cm^{-1} and 400 cm^{-1}, which belong to Ge–Ge and Si–Ge Raman active modes, respectively. There are no obvious Si–Si peaks near 500 cm^{-1}, probably because of the much lower concentration of Si than that of Ge in the samples. The asymmetric shapes of these peaks are caused by the amorphous phase. The sharper Ge–Ge phonon mode and Si–Ge phonon mode in S2 confirm that the annealed sample (S2) has better crystalline quality than the as-grown one (S1). The blue shift of the Ge–Ge phonon mode compared to that of the Ge substrate (300.5 cm^{-1}) could be caused by the Mn–Ge alloy formation,[17] Si–Ge alloy polycrystalline nature, or tensile strain,[22] so it is quite difficult to distinguish them from each other by Raman spectroscopy.

To investigate the elementary distribution in the annealed sample S2, the high-angle annular-dark-field (HAADF) image and EDS-mappings for Si, Ge, and Mn were obtained. It shows that the Si and Ge elements were homogeneously distributed, but the Mn elements were not. Similar results were observed in the heavily (above 8%) Mn-doped GaAs grown by low temperature molecular epitaxy, owing to the high concentration and low solubility of the Mn element.[1–3] The inhomogeneous distribution of the Mn elements implies that the Mn-related secondary phases may be formed in the annealed samples, which is consistent with the finding of the GIXRD.

Further structural characterizations were performed by using high-resolution TEM (HRTREM). Figures 2(d)–2(f) show the HRTEM images of samples S1, S2, and S3, and the corresponding fast Fourier transform (FFT) patterns are shown in Figs. 2(a)–2(c). A typical amorphous ring can be seen in Fig. 2(a), which indicates the amorphous phase in the as-grown sample (S1). After annealing, the diffraction ring becomes clear, which indicates the improvement in the crystalline of the SiGe phase. Comparing the results of the annealed samples S2 and S3, clearer sharp diffraction rings (220) and (331) can be seen in sample S3. Meanwhile, there were also some other phases detected in the annealed samples (marked as 01, 02, and 03). Comparing to the unstrained (111) plane spacing (0.323 nm) of $Si_{0.25}Ge_{0.75}$, the (111) plane spacing marked in Figs. 2(e) and 2(f) (0.334 nm and 0.336 nm for samples S2 and S3, respectively) reveals the tensile strain inside the SiGe phase. Considering that the atomic radius of the dopant Mn (1.61 Å) is larger than that of Si (1.11 Å) and Ge (1.25 Å), the tensile strain detected inside the SiGe phase could be resulted from the Mn incorporation in the lattice matrix[23] apart from the Ge substrate.

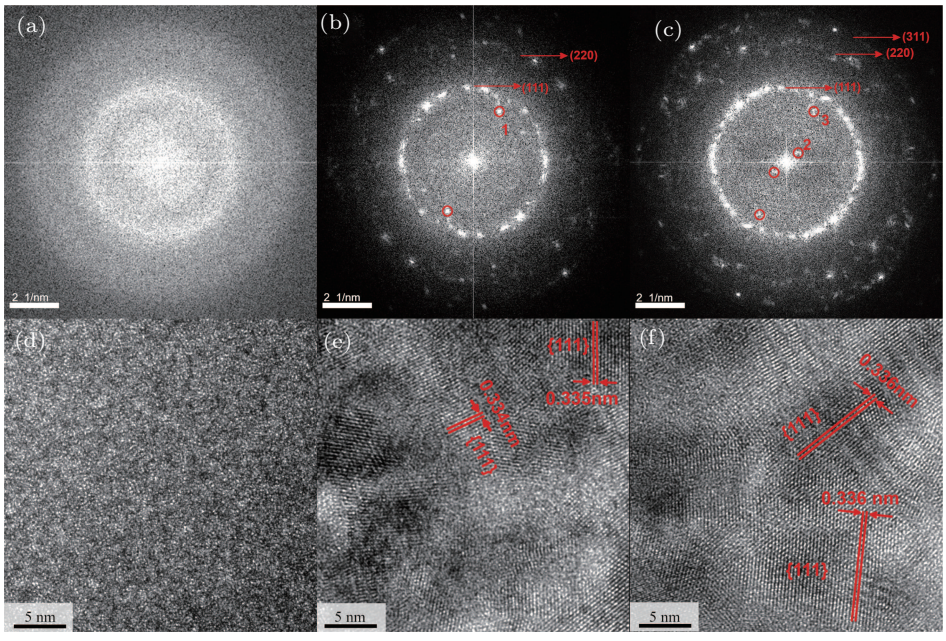


Fig. 2. HRTEM images of samples (d) S1, (e) S2, and (f) S3; and the corresponding FFT patterns for (a) S1, (b) S2, and (c) S3.

Considering the possible combinations of various kinds of manganese silicide and manganese germanide nanostructures in the alloy background, it is not easy to identify these nanoclusters. We found by using HRTEM that most of the nanoclusters were surrounded by amorphous phase and the diameters of these nanoclusters varied from 10 nm to 20 nm. Figure 3 shows a typical secondary phase in sample S3. The crystalline area of the nanocluster (red border) shown in Fig. 3(a) was analyzed by FFT shown in Fig. 3(b). The reflections in the diffractogram of the FFT marked as 01 and 02 reveal two plane spacings of 0.233 nm and 0.617 nm. They are consistent with the characteristic spacings of 0.235 nm

and 0.622 nm for the (210) and (100) planes of the Ge_3Mn_5 structure (PDF# 89-4887), which has also been detected in the GIXRD measurements.

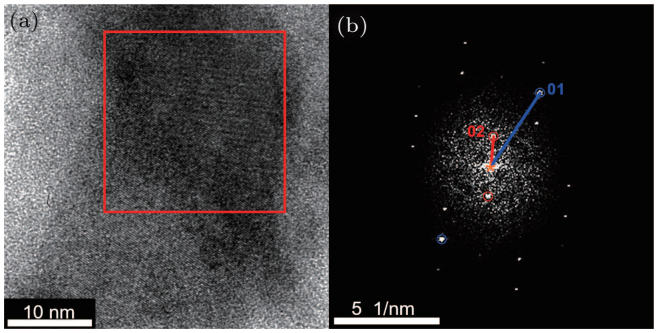


Fig. 3. (a) HRTEM image of a typical secondary Ge_3Mn_5 nanocluster in sample S3. (b) The corresponding FFT analysis image for the crystalline phase.

The magnetic properties of the samples were measured by SQUID. Figure 4(a) shows the temperature dependence of zero-field cooling (ZFC) and field cooling (FC) magnetization for samples S1, S2, and S3 at 20 Oe. Under ZFC condition, the sample was cooled down to 5 K in zero field, then heated up to high temperature with an applied magnetic field. While for the FC process, the sample was firstly cooled down to 5 K with an applied magnetic field, then heated up with the same field. As shown in Fig. 4(a), the as-grown sample S1 exhibited weak ferromagnetism with a T_C at about 50 K, while the annealed samples S2 and S3 exhibited stronger ferromagnetism and there appeared splitting between their ZFC and FC curves. It is worth noting that pure Ge is diamagnetic and pure Mn is antiferromagnetic (AFM). As to the manganese oxides, most of them are AFM except that Mn_3O_4 shows ferromagnetism with a T_C at about 42 K,[24] but no Mn_3O_4 phase was detected in our measurements. In the SiMn system, the energetically favorable manganese silicide phase is $MnSi_{1.7}$ (Mn_4Si_7, $Mn_{11}Si_{19}$, or $Mn_{15}Si_{26}$), which exhibits a weak itinerant ferromagnetism below 50 K and shows a dramatic decrease in ZFC magnetization curve below 25 K.[13,14] These features were not observed in our samples. Importantly, in the GeMn system, Mn-rich clusters such as Ge_3Mn_5 and Ge_8Mn_{11} are the most common clusters,[25–27] in which Ge_3Mn_5 shows a T_C at around 300 K[26] and Ge_8Mn_{11} shows an FM ordering between 150 K and 285 K and an AFM ordering below 150 K.[26,27] Since the T_C defined by the differentiation of magnetization over temperature for samples S2 and S3 were 285 K and 305 K, respectively, the ferromagnetism at the higher temperature around 300 K was probably contributed by the Ge_3Mn_5 nanoclusters. However, we could not completely exclude other contributions to the ferromagnetism since there were still unknown phases in our samples. It is interesting that the T_C was slightly improved by increasing the Mn concentration in the annealed samples. Meanwhile, the unsmooth FC curves and the slowly increasing FC curves at the lower temperature indicate that there existed extra FM contributions from the tensile-strained Mn diluted SiGe matrix[19] in the annealed samples. The previous study indicated that tensile-strain can enhance the ferromagnetism in Mn diluted group-IV semiconductors.[28] The measurements of the magnetization versus magnetic field curves also confirm the FM ordering in the annealed samples S2 and S3. Figure 4(b) shows the result of a typical sample S2 at different temperatures, where the diamagnetic signal from the Ge substrate has been subtracted. The *M*–*H* curves show hysteresis loops, which clearly indicate the ferromagnetism in the annealed samples. A weak FM signal was still shown at room temperature, which probably came from the Ge_3Mn_5 clusters in the annealed samples.

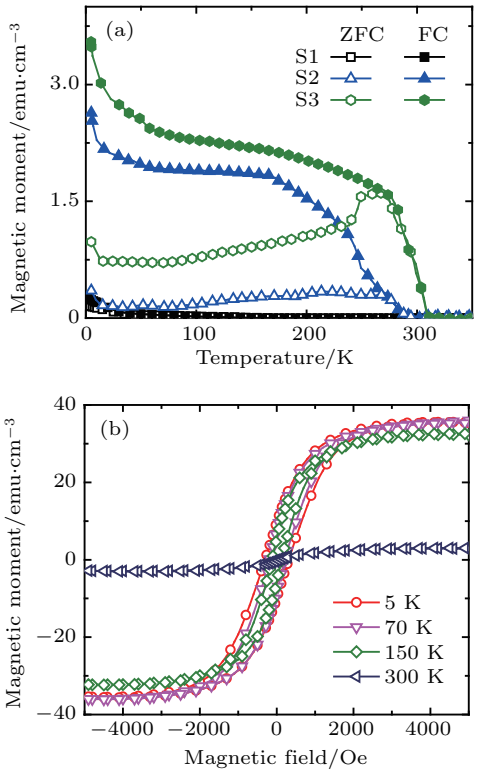


Fig. 4. (a) Temperature dependence of ZFC and FC magnetization for samples S1, S2, and S3. (b) *M*–*H* curves for sample S2.

4. Conclusion

In summary, heavily Mn-doped $Si_{0.25}Ge_{0.75}$ thin films were fabricated by using magnetron sputtering and post-growth annealing. Both Mn diluted SiGe crystals and Mn-rich nanoclusters were detected in the annealed samples owing to the high Mn concentration above 10%. The annealed samples showed a T_C above room temperature which was probably caused by the Ge_3Mn_5 nanoclusters. The results could be potentially useful for spintronic applications based on group IV materials.

Acknowledgment

We are very grateful to the help from the Analytical and Testing Center of Sichuan University.

References

[1] Ohno H, Shen A, Matsukura F, Oiwa A, Endo A, Katsumoto S and Iye Y 1996 *Appl. Phys. Lett.* **69** 363

[2] Chen L, Yang X, Yang F, Zhao J, Misuraca J, Xiong P and Von Molnár S 2011 *Nano Lett.* **11** 2584

[3] Wang M, Campion R P, Rushforth A W, Edmonds K W, Foxon C T and Gallagher B L 2008 *Appl. Phys. Lett.* **93** 132103

[4] Xiang G, Holleitner A W, Sheu B L, Mendoza F M, Maksimov O, Stone M B, Schiffer P, Awschalom D D and Samarth N 2005 *Phys. Rev. B* **71** 241307

[5] Venkatesan M, Fitzgerald C B, Lunney J G and Coey J M D 2004 *Phys. Rev. Lett.* **93** 177206

[6] Qi S, Jiang F, Fan J, Wu H, Zhang S B, Gehring G A, Zhang Z and Xu X 1951 *Phys. Rev. B* **84** 1

[7] Park Y D, Hanbicki A T, Erwin S C, Hellberg C S, Sullivan J M, Mattson J E, Ambrose T F, Wilson A, Spanos G and Jonker B T 2002 *Science* **295** 651

[8] Bolduc M, Awo-Affouda C, Stollenwerk A, Huang M B, Ramos F G, Agnello G and LaBella V P 2005 *Phys. Rev. B* **71** 033302

[9] Deng Z, Jin C Q, Liu Q Q, Wang X C, Zhu J L, Feng S M, Chen L C, Yu R C, Arguello C, Goko T, Ning F, Zhang J, Wang Y, Aczel A A, Munsie T, Williams T J, Luke G M, Kakeshita T, Uchida S, Higemoto W, Ito T U, Gu B, Maekawa S, Morris G D and Uemura Y J 2011 *Nat. Commun.* **2** 422

[10] Zhao K, Deng Z, Wang X C, Han W, Zhu J L, Li X, Liu Q Q, Yu R C, Goko T, Frandsen B, Liu L, Ning F, Uemura Y J, Dabkowska H, Luke G M, Luetkens H, Morenzoni E, Dunsiger S R, Senyshyn A, Böni P and Jin C Q 2013 *Nat. Commun.* **4** 1442

[11] Peng Y, Yu S, Zhao G Q, Li W M, Zhao J F, Cao L P, Wang X C, Liu Q Q, Zhang S J, Yu R Z, Deng Z, Zhu X H and Jin C Q 2019 *Chin. Phys. B* **28** 057501

[12] Woodbury H H and Tyler W W 1955 *Phys. Rev.* **100** 659

[13] Zhou S, Potzger K, Zhang G, Mücklich A, Eichhorn F, Schell N, Grötzschel R, Schmidt B, Skorupa W, Helm M, Fassbender J and Geiger D 1949 *Phys. Rev. B* **75** 1

[14] Aronzon B A, Davydov A B, Vasiliev A L, Perov N S, Novodvorsky O A, Parshina L S, Presniakov M Y and Lahderanta E 2017 *J. Phys. Condens. Matter* **29** 055802

[15] Jamet M, Barski A, Devillers T, Poydenot V, Dujardin R, Bayle-Guillemaud P, Rothman J, Bellet-Amalric E, Marty A, Cibert J, Mattana R and Tatarenko S 2006 *Nat. Mater.* **5** 653

[16] Ottaviano L, Passacantando M, Picozzi S, Continenza A, Gunnella R, Verna A, Bihlmayer G, Impellizzeri G and Priolo F 2006 *Appl. Phys. Lett.* **88** 061907

[17] Liu C, Hübner R, Xie Y, Wang M, Xu C, Jiang Z, Yuan Y, Li X, Yang J, Li L, Weschke E, Prucnal S, Helm M and Zhou S 2019 *Nanotechnology* **30** 054001

[18] Nie T, Tang J, Kou X, Gen Y, Lee S, Zhu X, He Q, Te L, Murata K, Fan Y and Wang K L 2016 *Nat. Commun.* **7** 12866

[19] Chen C H, Niu H, Yan D C, Hsieh H H, Lee C P and Chi C C 2012 *Appl. Phys. Lett.* **100** 242412

[20] Chu M, Sun Y, Aghoram U and Thompson S E 2009 *Annu. Rev. Mater. Res.* **39** 203

[21] Ferri F A and Zanatta A R 2009 *J. Phys. D. Appl. Phys.* **42** 035005

[22] Meyer F, Zafrany M, Eizenberg M, Beserman R, Schwebel C and Pellet C 1991 *J. Appl. Phys.* **70** 4268

[23] Cho S, Choi S, Hong S C, Kim Y, Ketterson J B, Kim B J, Kim Y C and Jung J H 2002 *Phys. Rev. B* **66** 033303

[24] Norton D P, Pearton S J, Hebard A F, Theodoropoulou N, Boatner L A and Wilson R G 2003 *Appl. Phys. Lett.* **82** 239

[25] Dietl T, Sato K, Fukushima T, Bonanni A, Jamet M, Barski A, Kuroda S, Tanaka M, Hai P N and Katayama-Yoshida H 2015 *Rev. Mod. Phys.* **87** 1311

[26] Biegger E, Stäheli L, Fonin M, Rüdiger U and Dedkov Y S 2007 *J. Appl. Phys.* **101** 103912

[27] Park Y D, Wilson A, Hanbicki A T, Mattson J E, Ambrose T, Spanos G and Jonker B T 2001 *Appl. Phys. Lett.* **78** 2739

[28] Weng H and Dong J 1947 *Phys. Rev. B* **71** 1